






Cite this: *Phys. Chem. Chem. Phys.*,
2018, 20, 25023

Excitonic phenomena in perovskite quantum-dot supercrystals

Ilia A. Vovk,  Nikita V. Tepliakov,  Anvar S. Baimuratov,  Mikhail Yu. Leonov, 
Alexander V. Baranov,  Anatoly V. Fedorov  and Ivan D. Rukhlenko  *

Quantum confinement and collective excitations in perovskite quantum-dot (QD) supercrystals offer multiple benefits to the light emitting and solar energy harvesting devices of modern photovoltaics. Recent advances in the fabrication technology of low dimensional perovskites has made the production of such supercrystals a reality and created a high demand for the modelling of excitonic phenomena inside them. Here we present a rigorous theory of Frenkel excitons in lead halide perovskite QD supercrystals with a square Bravais lattice. The theory shows that such supercrystals support three bright exciton modes whose dispersion and polarization properties are controlled by the symmetry of the perovskite lattice and the orientations of QDs. The effective masses of excitons are found to scale with the ratio of the superlattice period and the number of QDs along the supercrystal edge, allowing one to fine-tune the electro-optical response of the supercrystals as desired for applications. We also calculate the conductivity of perovskite QD supercrystals and analyze how it is affected by the optical generation of the three types of excitons. This paper provides a solid theoretical basis for the modelling of two- and three-dimensional supercrystals made of perovskite QDs and the engineering of photovoltaic devices with superior optoelectronic properties.

Received 25th July 2018,
Accepted 17th September 2018

DOI: 10.1039/c8cp04724c

rsc.li/pccp

1 Introduction

Over the past few years, lead halide perovskites (LHPs) have proven themselves as a promising material base for optoelectronic devices such as bright light sources^{1–6} and highly efficient solar cells.^{7–10} Of particular interest are nanocrystalline perovskites in the form of colloidal quantum dots (QDs), which are routinely synthesized these days by ligand-assisted reprecipitation (LARP) and other techniques.^{11–13} For example, achiral perovskite QDs can be used as an inexpensive gain medium for lasing^{6,14} while chiral ones¹⁵ are beneficial for various applications in biomedicine, spintronics, and catalytic chemistry.^{16,17} A unique feature of LHP QDs is their bright narrow-band photoluminescence, which is tunable over the entire visible^{12,13,18} and near-IR^{19,20} domains, highly defect tolerant,^{11,21} and has quantum yields of up to 100%.^{22,23} This feature has been recently explained by the existence of a highly emissive triplet state which informs the behaviour of the lowest-energy exciton of LHPs.^{24,25}

Perovskite QDs can be used as building blocks of perovskite QD supercrystals,²⁶ where their interaction leads to the collective supercrystal response to optical excitation.^{27–30} Such supercrystals can be fabricated by self-organisation,³¹ nanolithography,³² transfer printing,³³ 3D printing,³⁴ DNA origami,³⁵ and other techniques. The flexibility in the design of perovskite QD supercrystals, due to

the ability to preset the size, shape, and composition of individual QDs as well as to alter their arrangement and spatial orientations, significantly expands the potential of perovskites for the engineering of optoelectronic devices with predesigned functions.^{36–41}

Despite the active research on perovskite QD supercrystals,^{26,42,43} a rigorous theoretical description of their electric and optical properties is still lacking. Here we fill this gap by developing a first quantum-mechanical theory of Frenkel excitons in LHP QD supercrystals with a square Bravais lattice. The bright triplet state of LHPs is taken into account by modelling the lowest-energy excited states of individual QDs as three electric dipoles oriented along the crystallographic axes. The developed theory is used to analyze the dispersion and effective masses of the supercrystal excitons for different QD orientations and different symmetries of the perovskite crystal lattice. We also calculate the electric conductivity of LHP QD supercrystals and analyze its tensorial and spectral properties for different symmetries and excitation regimes of the supercrystal. This paper lays the theoretical foundation for the description of optoelectronic properties of two- and three-dimensional supercrystals made of perovskite QDs and may prove useful for the design of advanced photovoltaics devices.

2 Results and discussion

2.1 General formalism

In order to provide a general background for the following discussions on the properties of perovskite QD supercrystals,

Information Optical Technologies Centre, ITMO University,
Saint Petersburg 197101, Russia. E-mail: rukhlenko.ivan@gmail.com

we review some of the basic ideas underlying the theory of molecular crystals that can be used for the description of collective electronic excitations (Frenkel excitons) in periodic arrays of QDs.⁴⁴ Consider a two-dimensional supercrystal made of N alike and equally oriented QDs arranged in a simple square lattice of period a (see Fig. 1). By assuming that the QD positions in the lattice are fixed, we can write the supercrystal Hamiltonian in the form

$$\hat{H} = \sum_{\mathbf{n}} \hat{H}_{\mathbf{n}} + \frac{1}{2} \sum'_{\mathbf{n}, \mathbf{m}} \hat{V}_{\mathbf{n}, \mathbf{m}}, \quad (1)$$

where $\mathbf{n} = (n_x, n_y, 0)$ and $\mathbf{m} = (m_x, m_y, 0)$ are the integer lattice vectors, $\hat{H}_{\mathbf{n}}$ is the Hamiltonian of isolated QD \mathbf{n} located at point $\mathbf{r}_{\mathbf{n}} = a\mathbf{n}$, $\hat{V}_{\mathbf{n}, \mathbf{m}}$ is the interaction potential of QDs \mathbf{n} and \mathbf{m} , and the prime at the summation sign indicates that the terms with $\mathbf{n} = \mathbf{m}$ should be omitted.

The first key point of the general formalism is the assumption that wave functions $\phi_{\mathbf{n}}^l$ and energies $W_{\mathbf{n}}^l$ of isolated QDs are known. The wave functions obey Schrödinger's equation $\hat{H}_{\mathbf{n}}\phi_{\mathbf{n}}^l = W_{\mathbf{n}}^l\phi_{\mathbf{n}}^l$ and are normalized according to the condition $\int \phi_{\mathbf{n}}^{l*} \phi_{\mathbf{n}}^{l'} d\tau = \delta_{ll'}$, where δ_{ij} is the Kronecker delta and the integral is evaluated out over the entire space occupied by the supercrystal. In what follows we shall be interested in dipole-allowed transitions from the ground state (vacuum) of electron-hole pairs to the first r_0 excited states of close or equal energies W_r^0 ($r = 1, 2, \dots, r_0$). Each transition is characterized by its matrix element $\mathbf{d}_r = \int \phi_{\mathbf{n}}^{r*} \hat{\mathbf{p}}_{\mathbf{n}} \phi_{\mathbf{n}}^0 d\tau$, which is determined by the electric dipole moment $\hat{\mathbf{p}}_{\mathbf{n}}$ of QD \mathbf{n} and is independent of the QD position due to the same orientation of all QDs. The excitation energy can be transferred between the QDs of the supercrystal through the Coulomb interaction⁴⁵ described by the dipole-dipole potential

$$\hat{V}_{\mathbf{n}, \mathbf{m}} = \frac{1}{\varepsilon} \left(\frac{\hat{\mathbf{p}}_{\mathbf{n}} \cdot \hat{\mathbf{p}}_{\mathbf{m}}}{|\mathbf{r}_{\mathbf{n}, \mathbf{m}}|^3} - \frac{3(\hat{\mathbf{p}}_{\mathbf{n}} \cdot \mathbf{r}_{\mathbf{n}, \mathbf{m}})(\hat{\mathbf{p}}_{\mathbf{m}} \cdot \mathbf{r}_{\mathbf{n}, \mathbf{m}})}{|\mathbf{r}_{\mathbf{n}, \mathbf{m}}|^5} \right), \quad (2)$$

where ε is the effective permittivity of the interacting QDs and $\mathbf{r}_{\mathbf{n}, \mathbf{m}} = \mathbf{r}_{\mathbf{n}} - \mathbf{r}_{\mathbf{m}}$.

Another key point of the general formalism employs the fact that the interaction between the QDs in a typical supercrystal is relatively weak for individual QDs to retain their electronic configurations upon the formation of the supercrystal. This is the so-called Heitler-London approximation⁴⁶ allowing one to represent the wave function of the ground state of the supercrystal as a product of the wave functions of the ground states of individual QDs. The translational symmetry of the supercrystal then suggests that the excited supercrystal state with one exciton of quasimomentum $\mathbf{q} = (q_x, q_y, 0)$ is described by the wave function of the form

$$\Phi_{\mathbf{q}}^s = \frac{1}{\sqrt{N}} \sum_{\mathbf{n}, r} a_r^s(\mathbf{q}) e^{i\mathbf{q} \cdot \mathbf{r}_{\mathbf{n}}} \phi_{\mathbf{n}}^r \prod_{\mathbf{m} \neq \mathbf{n}} \phi_{\mathbf{m}}^0, \quad (3)$$

where s distinguishes between the exciton modes and $|a_1^s|^2 + |a_2^s|^2 + \dots + |a_{r_0}^s|^2 = 1$. The assumption of weak interdot coupling also implies the absence of tunneling of electrons and holes between the neighbouring QDs. This is always the case for QDs that are well separated by sufficiently long ligands.

The above assumptions allow one to reduce Schrödinger's equation $\hat{H}\Phi_{\mathbf{q}}^s = W_s\Phi_{\mathbf{q}}^s$ of the supercrystal as a whole to the following eigensystem problem for eigenvectors a_r^s and eigenvalues W_s :²⁷ $\sum_{r'} \Gamma_{rr'} a_{r'}^s = (W_s - W_0 - \Delta_r) a_r^s$, where W_0 is the ground-state energy of the supercrystal (its value is insignificant for the following discussions, because all physical quantities depend on difference $W_s - W_0$), $\Delta_r = W_r^0 - W_0^0$ is the excitation energy of an isolated QD, $\Gamma_{rr'} = \sum' M_{0,\mathbf{m}}^{rr'} \cos(\mathbf{q} \cdot \mathbf{r}_{\mathbf{m}})$, and $M_{\mathbf{n}, \mathbf{m}}^{rr'} = \int \phi_{\mathbf{n}}^{r*} \phi_{\mathbf{m}}^{0*} \hat{V}_{\mathbf{n}, \mathbf{m}} \phi_{\mathbf{n}}^0 \phi_{\mathbf{m}}^{r'} d\tau$ is the matrix element of the excitation exchange between QDs \mathbf{n} and \mathbf{m} . This eigensystem problem determines the wave functions and energies of r_0 exciton modes of the QD supercrystal.

2.2 Exciton modes of perovskite supercrystals

Perovskite QDs have three lowest-energy electric dipole transitions with dipole moments directed along the three Cartesian axes,^{24,25} i.e. $\mathbf{d}_r = d_r \mathbf{e}_r$ ($r = x, y, z$). As a consequence, perovskite QD

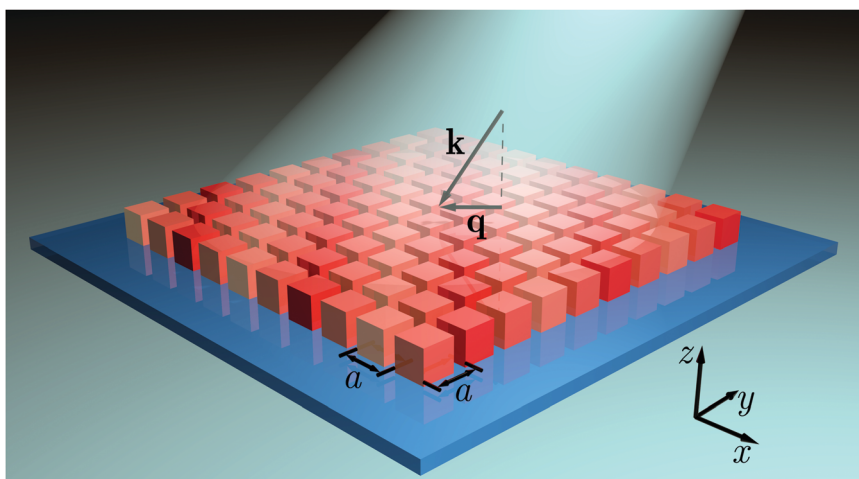


Fig. 1 Two-dimensional QD supercrystal with a square Bravais lattice of period a and exciton of quasimomentum \mathbf{q} excited in the supercrystal by incident light of wave vector \mathbf{k} .

supercrystals are characterized by the symmetric interaction matrix

$$\Gamma_{rr'}(\mathbf{q}) = \frac{d_r d_{r'}}{\varepsilon a^3} \sum_{\mathbf{m} \neq 0} \left(\frac{\delta_{rr'}}{|\mathbf{m}|^3} - \frac{3m_r m_{r'}}{|\mathbf{m}|^5} \right) \cos(\mathbf{q} \cdot \mathbf{r}_m), \quad (4)$$

whose diagonal components are related by the equation $\Gamma_{xx}d_x^{-2} + \Gamma_{yy}d_y^{-2} + \Gamma_{zz}d_z^{-2} = 0$.

The absence of energy exchange between the z-polarized dipoles and the in-plane dipoles \mathbf{d}_x and \mathbf{d}_y results in the decoupling of the z-polarized excitons from the excitons polarized in the plane of the supercrystal ($\Gamma_{zx} = \Gamma_{zy} = 0$). Using this fact to solve the eigensystem problem yields the following three exciton modes of perovskite QD supercrystals:

$$W_z = W_0 + \Gamma'_z, \quad a_x^\pm = a_y^\pm = 0, \quad a_z^\pm = 1, \quad (5)$$

$$W_\pm = W_0 + \frac{1}{2} \left(\Gamma'_x + \Gamma'_y \pm \sqrt{(\Gamma'_x - \Gamma'_y)^2 + 4\Gamma_{xy}^2} \right), \quad (6)$$

$$a_x^\pm = \pm a_y^\pm = \pm \sqrt{\frac{1}{2} \left(1 \pm \frac{G}{\sqrt{G^2 + 1}} \right)}, \quad a_z^\pm = 0, \quad (7)$$

where $\Gamma'_r = \Gamma_{rr} + \Delta_r$ and $G = (\Gamma'_x - \Gamma'_y) / (2|\Gamma_{xy}|)$. Eqn (4)–(6) show that the excitons' dispersion scales as $\propto a^{-3}$.

The obtained expressions describe two distinct exciton regimes which are related to different coupling strengths of the x- and y-polarized dipoles. The regime of strong coupling occurs when $|\Gamma_{xy}| \gg |\Gamma'_x - \Gamma'_y|$ and refers to situations where the \pm exciton modes are a mixture of collective excitations of the two orthogonal polarizations. It can be observed in the vicinity of degenerate points \mathbf{q}_0 determined by the condition $\Gamma'_x(\mathbf{q}_0) = \Gamma'_y(\mathbf{q}_0)$. At these points $W_\pm = W_0 + \Gamma'_x \pm |\Gamma_{xy}|$, $a_x^\pm = \pm a_y^\pm \approx \pm 1/\sqrt{2}$, and exciton wave functions $\Phi_{\mathbf{q}_0}^\pm$ are symmetric (+) or antisymmetric (−) with respect to the permutation of the x- and y-polarized dipoles. The weak coupling regime occurs when $|\Gamma'_x - \Gamma'_y| \gg |\Gamma_{xy}|$ and describes situations where the energy exchange between the x- and y-polarized dipoles can be ignored. This regime exists near degenerate points $\Gamma_{xy}(\mathbf{q}_0) = 0$ and is characterized by almost 'independent' modes of energies $W_x \approx W_0 + \Gamma'_x$ and $W_y \approx W_0 + \Gamma'_y$, which correspond to the collective excitations of different polarizations ($a_x^\pm = a_y^\pm \approx 1$, $a_z^\pm \approx 0$).

In what follows we focus on CsPbX₃ QDs with X = Cl, Br, or I. Their three excited states have equal oscillator strengths^{24,47} $2m_0 d_r^2 \Delta_r / (\hbar e)^2$ (m_0 is the free-electron mass), which in the case of close energies Δ_r implies that the three transition dipole moments are equal ($d_x = d_y = d_z = d$). With this simplification, our further analysis of CsPbI₃ QD supercrystals requires the knowledge of three quantities: Γ_{zz} , $\Gamma_{xx} - \Gamma_{yy}$, and Γ_{xy} .

2.3 Excitons in supercrystals of different symmetries

The degeneracy of the excited states of individual QDs is determined by the symmetry of the QD crystal lattice. Perovskites typically

belong to the orthorhombic (D_{2h}), tetragonal (D_{4h}), or cubic (O_h) lattice system.¹² The cubic and orthorhombic systems correspond to $\Delta_x = \Delta_y = \Delta_z$ and $\Delta_x \neq \Delta_y \neq \Delta_z$, respectively, whereas the tetragonal system corresponds to a nondegenerate low-energy QD state and a pair of doubly degenerate high-energy states,^{24,48} e.g. $\Delta_x = \Delta_y > \Delta_z$.

The symmetry of the supercrystal as a whole depends on both the symmetry and orientation of individual QDs. This symmetry is C_{4v} if the supercrystal QDs have equal transition energies in the xy plane ($\Delta_x = \Delta_y$) and C_{2v} in all other cases. In order to distinguish between the supercrystals with different orientations of the QDs, we introduce a superscript in the notation of the QD symmetry indicating the direction(s) of the lowest-energy dipole transition(s). For example, D_{2h}^{zx} denotes a supercrystal made of orthorhombic perovskite QDs with the lowest-energy electric dipole transitions along the z and x axes. Note that supercrystals with opposite signs of difference $\Delta_y - \Delta_x$ are alike, because they are mirror images of each other upon the reflection in planes $y = \pm x$.

Fig. 2 shows exciton energies in six CsPbI₃ supercrystals of different configurations. For O_h symmetry of the QD lattice energies W_+ and W_- coincide at points Γ and M , where $\Gamma_{xx} = \Gamma_{yy}$ and $\Gamma_{xy} = 0$. The lowering of the QD symmetry from O_h down to D_{4h} and D_{2h} (except for D_{4h}^{zz}) lowers the symmetry of the supercrystal from C_{4v} to C_{2v} and modifies its exciton dispersion. The parts of the \pm dispersion branches along the symmetry lines Δ and Z (where $\Gamma_{xy} = 0$) shift parallel to themselves, whereas the degenerate point at the Brillouin zone center splits into two points located symmetrically with respect to Γ on line Δ for $\Delta_y > \Delta_x$ (or Δ' for $\Delta_x > \Delta_y$). At the same time, the degenerate points at the four corners of the first Brillouin zone shift along the symmetry line Z (or Z') and merge with the other two degenerate points at points X (or X') for $\Delta_y - \Delta_x \approx \pm 11.1d^2/(ea^3)$ (not shown). Both dispersion branches modify more significantly along the symmetry lines Σ (where $|\Gamma_{xy}|$ peaks), acquiring almost identical shapes in supercrystal D_{2h}^{xz} with $\Delta_y - \Delta_x \approx 6$ meV due to the wakening of the coupling between the x- and y-polarized excitons.

In sharp contrast to the \pm excitons, the z dispersion branch is not affected by the symmetry of the supercrystal lattice. This branch shifts as a whole as the symmetry of the QD lattice changes, leading to the displacement of degenerate energies at the intersection of bands W_z and W_\pm according to the equation $(\Gamma'_x - \Gamma'_z)(\Gamma'_y - \Gamma'_z) = \Gamma_{xy}^2$.

2.4 Effective masses of excitons

Suppose that our supercrystal is excited by a monochromatic plane wave of frequency ω and wave vector $\mathbf{k} = k(\sin \theta \cos \phi, \sin \theta \sin \phi, -\cos \theta)$, where θ and ϕ are the polar angle and azimuth of the incidence direction. The conservation of crystal momentum requires the quasimomentum of generated excitons to be equal to the in-plane component of the absorbed photon wave vector,⁴⁶ $\mathbf{k}_{||} = (k_x, k_y, 0)$. Since the period of the supercrystal lattice is much smaller than the excitation wavelength, the optical response of the supercrystal is determined by the exciton dispersion near the Brillouin zone centre, i.e. by $|\mathbf{q}| \ll \pi/a$.

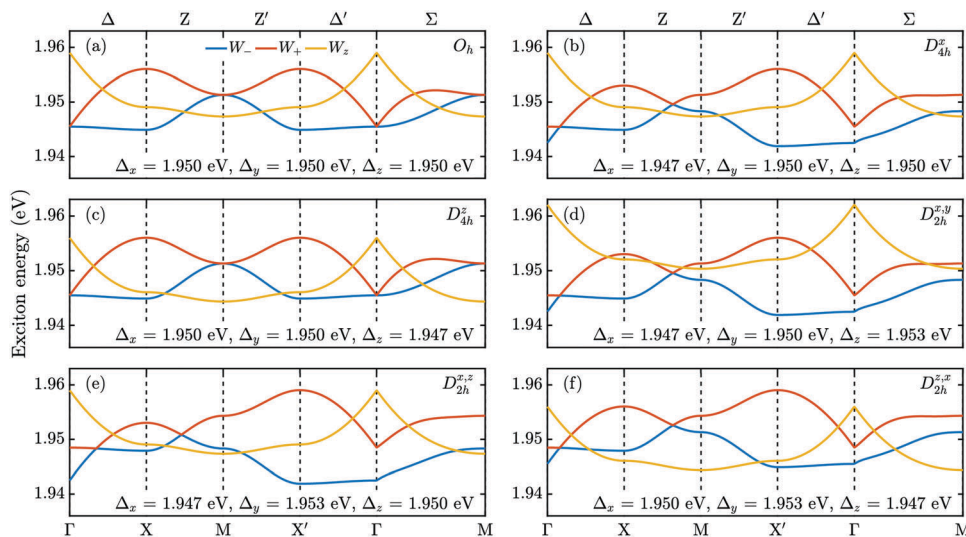


Fig. 2 Energies of excitons in CsPbI₃ QD supercrystals for different symmetries and orientations of QDs shown in the right top corners of the panels. Excitation energies of QDs are shown at the bottoms of the panels; $d = 52$ D, $\epsilon = 5$, and $a = 7$ nm.^{24,28} Points X and X' refer to $\mathbf{q} = (\pi/a)\mathbf{e}_x$ and $\mathbf{q} = (\pi/a)\mathbf{e}_y$, respectively.

Eqn (4)–(6) show that the energy of excitons near point Γ of an infinitely large supercrystal is a linear function of wave vector, $W_s \approx w_s|\mathbf{q}|$; here coefficients w_{\pm} depend on ϕ and the symmetry of the supercrystal, which is especially evident along the symmetry line Σ (Fig. 2). The linear dispersion law implies that excitons in infinite perovskite supercrystals are massless.⁴⁹ The dispersion of exciton in real supercrystals deviates from the linear one, resulting in small yet finite exciton masses. These masses need to be taken into account when the size of the supercrystal is comparable to or smaller than the exciton wavelength $\lambda_{\parallel} = \lambda/\sin \theta$. It should be noted that in the calculation of the effective masses of the \pm excitons in supercrystals of symmetry C_{2v} one can ignore the degenerate points of the energy spectrum, because these points lie outside the area $|\mathbf{q}| \ll \pi/a$ and do not affect the optical properties of the supercrystals.

Suppose that our supercrystal is a $(2M+1) \times (2M+1)$ square array of QDs and that its lateral dimensions are smaller than $\lambda_{\parallel}/2$. Then the cosine in eqn (4) can be approximated by the first two terms in its Taylor series expansion near the Brillouin zone centre and the interaction matrix of the supercrystal takes the form

$$\Gamma_{rr'}^{(M)}(\mathbf{q}) \approx \Gamma_{rr'}^{(M)}(\mathbf{0}) - \frac{d^2}{2\epsilon a} \sum_{\mathbf{m} \neq \mathbf{0}}^{|m_{x,y}| \leq M} \left(\frac{\delta_{rr'}}{|\mathbf{m}|^3} - \frac{3m_r m_{r'}}{|\mathbf{m}|^5} \right) (\mathbf{q} \cdot \mathbf{m})^2. \quad (8)$$

By replacing here summation by integration and evaluating the integrals, we find

$$\Gamma_{zz}^{(M)}(\mathbf{q}) - \Gamma_{zz}^{(M)}(\mathbf{0}) \approx -AM\kappa(q_x^2 + q_y^2), \quad (9)$$

$$\Gamma_{xx}^{(M)}(\mathbf{q}) - \Gamma_{yy}^{(M)}(\mathbf{q}) \approx BM\kappa(q_x^2 - q_y^2), \quad (10)$$

$$\Gamma_{xy}^{(M)}(\mathbf{q}) \approx 2\sqrt{2}M\kappa q_x q_y, \quad (11)$$

where $A = 2 \operatorname{arsinh} 1$, $B = 3A - 2\sqrt{2}$, and $\kappa = d^2/(\epsilon a)$. The obtained expressions are applicable when the number of QDs in a row are smaller than $\lambda_{\parallel}/(2a)$.

Eqn (5), (6) and (9)–(11) assume certain effective masses of the supercrystal excitons. It is easy to see that the inverse effective-mass tensor⁵⁰ $m_{s,ij}^{-1} = \hbar^{-2} \partial_{q_i}^2 W_s$ is proportional to the ratio $\kappa M/\hbar^2$, which will be used as the units of measure of tensor components for the sake of convenience. In these units, the z-polarized excitons are characterized by the negative scalar effective mass $m_z^{-1} = -2A$.

The excitons of energies W_{\pm} have tensorial effective masses, which depend on the symmetry of the supercrystal. In supercrystals of symmetry C_{2v} [see Fig. 2(b) and (d–f)] the inverse effective-mass tensor is diagonal and given by $m_{\pm,ij}^{-1} = [A \pm (-1)^{\delta_{ij}} B \operatorname{sign}(\Delta_x - \Delta_y)]\delta_{ij}$. Its two components have opposite signs and are independent of the absolute value of energy splitting $\Delta_x - \Delta_y$. The excitons of energy W_+ (W_-) possess the positive effective mass $A + B$ when their quasimomentum is aligned to the dipole moment of transition to the higher-energy (lower-energy) excited state of the QDs.

The situation is more complicated for supercrystals of symmetry C_{4v} [see Fig. 2(a and c)]. In this case exciton masses are anisotropic and characterized by the tensor

$$m_{\pm,ij}^{-1} = \left(A \pm \frac{8 - (-1)^{\delta_{ij}} C \cos^3 2\phi}{(8 - C \cos^2 2\phi)^{3/2}} B^2 \right) \delta_{ij} \pm \frac{8C \sin^3 2\phi}{(8 - C \cos^2 2\phi)^{3/2}} (1 - \delta_{ij}), \quad (12)$$

where $C = 8 - B^2$ and $\phi = \arctan(q_y/q_x)$. The components of this tensor are plotted in Fig. 3. One can see that the diagonal components of the two exciton modes have opposite signs, $m_{+,ii}^{-1} > 0$ and $m_{-,ii}^{-1} < 0$. The largest inverse effective masses $A \mp B \pm 16/B$ belong to excitons propagating along the supercrystal axes whereas the smallest diagonal masses $A \pm 2^{-3/2}B^2$ correspond to the propagation directions $\phi = \pm\pi/4$ and $\pm 3\pi/4$.

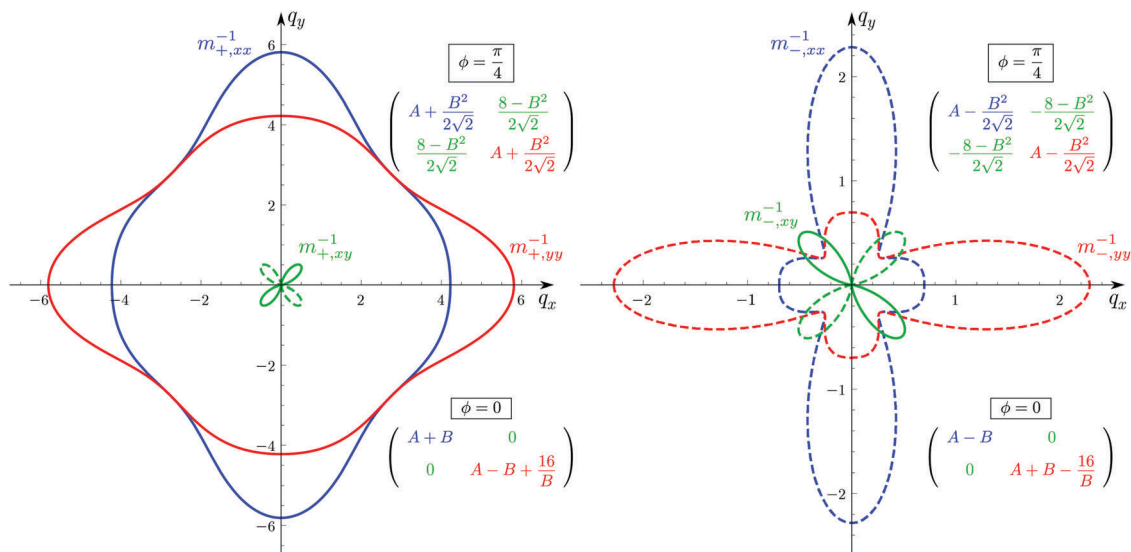


Fig. 3 Components xx (blue), yy (red), and xy (green) of inverse effective mass tensor of $+$ (left) and $-$ (right) exciton modes in perovskite QD supercrystals of symmetry C_{4v} . Negative values are shown by dashed curves.

2.5 Conductivity of perovskite supercrystals

The results of the previous sections allow one to calculate the linear electrical conductivity $\sigma_{ij}(\omega, \mathbf{k})$ of perovskite QD supercrystals, which relates the electric field $\mathbf{E}(\omega, \mathbf{k})$ of the incident electromagnetic wave to the current density $\mathbf{j}(\omega, \mathbf{k})$ induced by it as $\mathbf{j} = \sigma \mathbf{E}$. In order to take into account the decay of the supercrystal excitons due to phonon scattering, we introduce decay rates γ_s of exciton modes and small shifts $\Delta\omega_s$ of mode frequencies $\omega_s = W_s/\hbar$ ($\Delta\omega_s \ll \omega_s$). The dipole-dipole interaction approximation then yields the supercrystal conductivity of the form⁴⁴

$$\sigma_{ij} = \frac{ie^2}{a^3\mu\omega}\delta_{ij} + \frac{i}{a^3\hbar\omega} \sum_s \left(\frac{1}{\omega - \tilde{\omega}_s + i\gamma_s} - \frac{1}{\omega + \omega_s} \right) D_{\mathbf{k}s}^i D_{\mathbf{k}s}^j \omega_s^2, \quad (13)$$

where μ is the reduced mass of electron-hole pairs in QDs, $\mathbf{D}_{\mathbf{k}s} = \sum_r a_r^s(\mathbf{k}) \mathbf{d}_r$ is the dipole moment of QDs in the s th exciton mode, and $\tilde{\omega}_s(\omega, \mathbf{k}) = \omega_s(\mathbf{k}) + \Delta\omega_s(\omega)$ is the exciton frequency. The pole at $\omega = 0$ can be conveniently eliminated using the relation $(e^2/\mu)\delta_{ij} = (2/\hbar) \sum D_{\mathbf{k}s}^i D_{\mathbf{k}s}^j \omega_s$ to get

$$\sigma_{ij} = \frac{i}{a^3\hbar} \sum_s \frac{2\omega + i(2 + \omega_s/\omega)\gamma_s}{(\omega - \tilde{\omega}_s + i\gamma_s)(\omega + \omega_s)} D_{\mathbf{k}s}^i D_{\mathbf{k}s}^j \omega_s. \quad (14)$$

For relatively narrow exciton resonances ($\gamma_s \ll \omega_s$) this equation can be simplified further by setting $i(2 + \omega_s/\omega)\gamma_s \approx 3i\gamma_s$.

According to its definition, $\gamma_s(\omega)$ is proportional to the transition rate of excitons from energy state $\hbar\omega_s$ to energy state $\hbar\omega$ due to the absorption or emission of phonons. Because this rate is significant only near the resonance frequency ω_s and tends to zero far away from this frequency, the supercrystal conductivity vanishes for $\omega = 0$.

The simple form of the dipole moment of perovskite QDs, $D_{\mathbf{k}s}^i = a_i^s(\mathbf{k})d$, allows one to consider separately the normal

component of the supercrystal conductivity $\sigma_{zz} = j_z/E_z$ ($\sigma_{zx} = \sigma_{zy} = 0$), which is induced by the z -polarized excitons, and the in-plane components induced by the \pm exciton modes. The in-plane components of the conductivity tensor as given by eqn (14) are the sums of contributions from the two exciton modes

$$\sigma_{\alpha\beta} = a_{\alpha}^+ a_{\beta}^+ \sigma^+ + a_{\alpha}^- a_{\beta}^- \sigma^-, \quad \alpha, \beta = x, y, \quad (15)$$

where σ^{\pm} are implicitly defined and $a_{\alpha}^+ a_{\beta}^+ = a_{\alpha}^- a_{\beta}^- = \delta_{\alpha\beta}$. Simple algebra shows that σ^{\pm} are the eigenvalues of $\sigma_{\alpha\beta}$ and hence give the maximal conductivities due to the excitation of the \pm modes. The corresponding eigenvectors (a_x^s, a_y^s) give the directions of the in-plane components of light polarizations required to excite each of the modes separately, and also the directions of the electric currents induced by such polarizations.

Let an optical wave generate excitons of zero quasimomentum upon the normal incidence onto the supercrystal. In this case the off-diagonal in-plane components of the conductivity tensor vanish, because $\Gamma_{xy}(\mathbf{0}) = 0$. For supercrystals of symmetry C_{2v} each of the diagonal components is contributed to by a single exciton peak, with a weight determined by the coefficient $(a_x^{\pm})^2 = [1 \pm \text{sign}(\Delta_x - \Delta_y)]/2$ or $(a_y^{\pm})^2 = 1 - (a_x^{\pm})^2$. The positions of the conductivity peaks are given by $\omega_{\pm} = \mathcal{G}_{xy}^{\pm} \tilde{\omega}_x + \mathcal{G}_{yx}^{\pm} \tilde{\omega}_y$, where $\tilde{\omega}_x = [\Delta_x - \Gamma_{zz}(\mathbf{0})/2]/\hbar + \Delta\omega_x$, $\Gamma_{zz}(\mathbf{0}) \approx 9d^2/(\epsilon a^3)$, $\mathcal{G}_{xy}^{\pm} = \mathcal{G}[\pm(\Delta_x - \Delta_y)]$, and $\mathcal{G}(x)$ is the Heaviside step function. In the special case of weakly coupled x - and y -polarized excitations the supercrystal conductivity takes the simple form $\sigma_{\alpha\beta} = \delta_{\alpha\beta} \sigma^z$. Supercrystals of symmetry C_{4v} have degenerate exciton modes at point Γ and are therefore characterized by isotropic conductivity ($\sigma_{xx} = \sigma_{yy}$). The in-plane components of the electric conductivity tensor are shown in Fig. 4.

The oblique incidence of light leads to the appearance of the off-diagonal components of the conductivity tensor and to the dependency of the conductivity tensor on the incidence

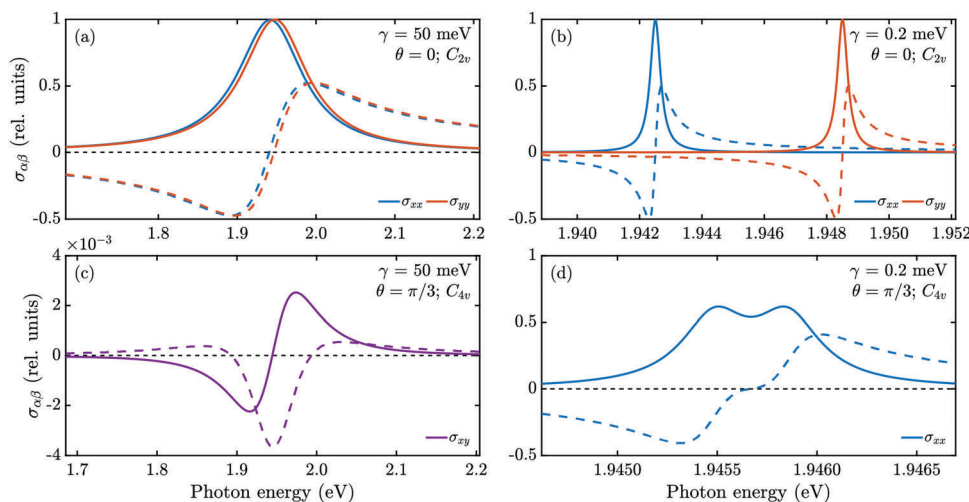


Fig. 4 In-plane components of electric conductivity tensor of CsPbI₃ QD supercrystals of different symmetries in the units of $d^2\Delta/(a^3\hbar^2\gamma)$. Left (right) panels refer to room (cryogenic) temperature and top (bottom) panels refer to normal (oblique) incidence. Real and imaginary parts are shown by solid and dashed curves, respectively. It was assumed that $\Delta = 1.95$ eV and $\phi = \pi/4$; the rest of simulation parameters are the same as in Fig. 2.

direction. By assuming that $\hbar\Delta\omega_{\pm} \ll W_+ - W_-$, setting $\gamma_+ = \gamma_- = \gamma$, and retaining the resonant terms in eqn (13), we obtain

$$\sigma_{xy} = \frac{id^2}{a^3\hbar} \frac{|\Gamma_{xy}|}{\hbar\omega} \frac{(\omega_+ + \omega_-)(\omega + i\gamma) - \omega_+\omega_-}{(\omega - \tilde{\omega}_+ + i\gamma)(\omega - \tilde{\omega}_- + i\gamma)}. \quad (16)$$

This conductivity vanishes when light propagates along the x or y axis, for which $\Gamma_{xy} = 0$. The peaks of $\text{Re}\sigma_{xy}$ are centered at frequencies $(\tilde{\omega}_+ + \tilde{\omega}_-)/2 \pm \gamma/\sqrt{3}$ when the decay rate is large compared to the exciton mode energy splitting, $\gamma \gg \tilde{\omega}_+ - \tilde{\omega}_-$, which is often the case at room temperatures.

We can estimate the relative size of the off-diagonal conductivity σ_{xy} by approximating Γ_{xy} near the Brillouin zone center as $\Gamma_{xy} \approx (\pi/\epsilon)(d/a)^2|\mathbf{k}_{\parallel}|\sin 2\phi$. The comparison of eqn (14) and (16) at the exciton resonance frequency then gives $|\sigma_{xy}|/|\sigma_{xx}| \sim (\pi/\epsilon)(d/a)^2|\mathbf{k}_{\parallel}|/(\hbar\gamma)$. This result shows that the off-diagonal conductivity is about three orders of magnitude smaller than the diagonal one for the parameters of Fig. 2, $\lambda = 700$ nm, and $\gamma = 50$ meV. The ratio $|\sigma_{xy}|/|\sigma_{xx}|$ grows with the reduction of temperature due to the decrease of γ as long as $\gamma \gg \tilde{\omega}_+ - \tilde{\omega}_-$. In the opposite limit of low temperatures and $\gamma \ll \tilde{\omega}_+ - \tilde{\omega}_-$ this ratio is independent of temperature and in supercrystals of symmetry C_{2v} has a maximal value of $(\pi/\epsilon)(d/a)^2|\mathbf{k}_{\parallel}|/|\Delta_x - \Delta_y|$, which is about 0.01 for the above parameters and $\Delta_x - \Delta_y = 3$ meV.

The diagonal and off-diagonal conductivities are comparable at low temperatures in supercrystals of symmetry C_{4v} . In these supercrystals TE waves excite the mode of energy W_- and induce the current $\mathbf{j} = \sigma^- \mathbf{E}_{\text{TE}}$ whereas TM waves excite the mode of energy W_+ and $\mathbf{j} = \sigma^+ \mathbf{E}_{\text{TM}}$. If the supercrystal is smaller than the exciton wavelength, *i.e.* $4Ma \lesssim \lambda_{\parallel}$, then Γ_{xy} in eqn (16) should be replaced with $\Gamma_{xy}^{(M)}$ [see eqn (11)], and the room-temperature estimate of the off-diagonal conductivity is reduced by a factor of $\lambda_{\parallel}/(2\sqrt{2}Ma)$.

The anisotropy of perovskite supercrystals upon the oblique excitation is most strongly manifested in the diagonal components

of the conductivity tensor. For example, the relative intensities of conductivity peaks σ^+ and σ^- in supercrystals of symmetry C_{4v} are determined by functions $(a_x^+)^2 = (a_y^-)^2 = \cos^2 \phi$ and $(a_x^-)^2 = (a_y^+)^2 = \sin^2 \phi$ [see eqn (15) and Fig. 4(d)]. The energy splitting of these peaks, equal to $2(\pi/\epsilon)(d/a)^2|\mathbf{k}_{\parallel}|$, is typically in the millielectronvolt range and can be observed at cryogenic temperatures. In the case of weakly coupled x - and y -polarized excitons the main peaks of σ_{xx} and σ_{yy} are accompanied by much weaker secondary peaks of $(2G)^{-2}$ times smaller intensities, which are independent of temperature.

The developed theory can be readily generalized to the case of three-dimensional (3D) perovskite QD supercrystals with a cubic lattice. In this case all the results of Section 2.1 and eqn (4) remain valid, provided that \mathbf{n} and \mathbf{m} are treated as three-dimensional integer lattice vectors. The major physical difference of 3D supercrystals from the 2D ones is that the three types of the orthogonal dipole moments are coupled to one another and the resulting exciton modes are fully mixed. From the mathematical viewpoint, the key difference between the 3D and 2D cases relates to the calculation of the conductivity tensor, which requires one to eliminate the contribution of a macroscopic field (which is irregular at point $\mathbf{k} = \mathbf{0}$) to the total Coulomb coupling of the dipoles. The elimination procedure is standard and discussed in detail in textbooks.⁵¹

As a concluding remark, we would like to reiterate that the present theory is only applicable in the absence of tunneling of electrons and holes between the QDs, *i.e.* when the interdot coupling can be described by eqn (2). The tunneling may occur between very closely spaced QDs due to the relatively small electron-hole binding energies of the perovskites. It leads to the separation of the electron-hole pairs across different neighboring QDs and changes the type of conductivity of the perovskite QD supercrystal. The conductivity type can also be affected by the disordering of the QDs in the superlattice. If this disordering is relatively weak, it leads to the scattering of

excitons by the lattice imperfections and can be described by the broadening of the conductivity peaks. On the other hand, strong disordering results in the disappearance of the collective excitations and essentially changes the conductivity of the supercrystal.

3 Conclusions

We have shown that two-dimensional supercrystals made of lead-halide perovskite QDs support three bright exciton modes, one of which is due to the electric dipole transitions perpendicular to the plane of the supercrystal while the other two are due to the transitions in this plane. If the perovskite lattice is cubic, then the supercrystal has symmetry C_{4v} and the coupling of its in-plane x - and y -polarized transitions yields excitons of 'mixed' polarizations. The lowering of the perovskite lattice symmetry that makes the energies of the in-plane transitions different lowers the symmetry of the supercrystal down to C_{2v} and can lead to the decoupling of the x - and y -polarized excitons if the energies of the in-plane transitions are significantly different. In supercrystals whose linear dimensions are smaller than or comparable to the exciton wavelength the effective masses of excitons are directly proportional to the superlattice period and inversely proportional to the number of QDs along the supercrystal edge and the transition dipole moment squared. We also showed that the eigenvalues of the complex conductivity tensor of perovskite QD supercrystals give the maximal conductivities due to the generation of the three types of excitons. The optical excitation of supercrystals of symmetry C_{2v} generates excitons whose dipole moments are parallel to the incident field polarization whereas in supercrystals of symmetry C_{4v} TE waves generate low-energy excitons W_- and TM waves generate high-energy excitons W_+ . The energy splitting of the exciton peaks in the supercrystal conductivity spectrum was found to be about several meV, which can be easily observed at cryogenic temperatures. These results will prove useful for engineering superior devices based on two- and three-dimensional perovskite QD supercrystals with controllable optoelectronic properties.

Conflicts of interest

There are no conflicts to declare.

Acknowledgements

This work was supported by the Russian Science Foundation (Agreement 18-13-00200) and by Grant MD-1294.2017.2 of the President of the Russian Federation for Young Scientists. The authors also thank the Ministry of Education and Science of the Russian Federation for its Projects 14.Y26.31.0028 and 16.8981.2017/8.9 and Scholarships SP-2066.2016.1 and SP-1975.2016.1.

Notes and references

- 1 A. Balena, A. Perulli, M. Fernandez, M. L. De Giorgi, G. Nedelcu, M. V. Kovalenko and M. Anni, *J. Phys. Chem. C*, 2018, **122**, 5813–5819.
- 2 H. Cho, J. S. Kim, C. Wolf, Y.-H. Kim, H. J. Yun, S.-H. Jeong, A. Sadhanala, V. Venugopalan, J. W. Choi, C.-L. Lee, R. H. Friend and T.-W. Lee, *ACS Nano*, 2018, **12**, 2883–2892.
- 3 C. Huang, W. Sun, Y. Fan, Y. Wang, Y. Gao, N. Zhang, K. Wang, S. Liu, S. Wang, S. Xiao and Q. Song, *ACS Nano*, 2018, **12**, 3865–3874.
- 4 L. Meng, E.-P. Yao, Z. Hong, H. Chen, P. Sun, Z. Yang, G. Li and Y. Yang, *Adv. Mater.*, 2017, **29**, 1603826.
- 5 S. Colella, M. Mazzeo, A. Rizzo, G. Gigli and A. Listorti, *J. Phys. Chem. Lett.*, 2016, **7**, 4322–4334.
- 6 S. Yakunin, L. Protesescu, F. Krieg, M. I. Bodnarchuk, G. Nedelcu, M. Humer, G. De Luca, M. Fiebig, W. Heiss and M. V. Kovalenko, *Nat. Commun.*, 2015, **6**, 8056.
- 7 J.-P. Correa-Baena, M. Saliba, T. Buonassisi, M. Grätzel, A. Abate, W. Tress and A. Hagfeldt, *Science*, 2017, **358**, 739–744.
- 8 G. E. Eperon, M. T. Hörantner and H. J. Snaith, *Nat. Rev. Chem.*, 2017, **1**, 0095.
- 9 W. S. Yang, B.-W. Park, E. H. Jung, N. J. Jeon, Y. C. Kim, D. U. Lee, S. S. Shin, J. Seo, E. K. Kim, J. H. Noh and S. I. Seok, *Science*, 2017, **356**, 1376–1379.
- 10 M. A. Green, A. Ho-Baillie and H. J. Snaith, *Nat. Photonics*, 2014, **8**, 506–514.
- 11 Q. A. Akkerman, G. Rainò, M. V. Kovalenko and L. Manna, *Nat. Mater.*, 2018, **17**, 394–405.
- 12 M. V. Kovalenko, L. Protesescu and M. I. Bodnarchuk, *Science*, 2017, **358**, 745–750.
- 13 I. Levchuk, A. Osvet, X. Tang, M. Brandl, J. D. Perea, F. Hoegl, G. J. Matt, R. Hock, M. Batentschuk and C. J. Brabec, *Nano Lett.*, 2017, **17**, 2765–2770.
- 14 Y. Xu, Q. Chen, C. Zhang, R. Wang, H. Wu, X. Zhang, G. Xing, W. W. Yu, X. Wang, Y. Zhang and M. Xiao, *J. Am. Chem. Soc.*, 2016, **138**, 3761–3768.
- 15 T. He, J. Li, X. Li, C. Ren, Y. Luo, F. Zhao, R. Chen, X. Lin and J. Zhang, *Appl. Phys. Lett.*, 2017, **111**, 151102.
- 16 N. V. Teplakov, I. A. Vovk, A. S. Baimuratov, M. Y. Leonov, A. V. Baranov, A. V. Fedorov and I. D. Rukhlenko, *J. Phys. Chem. Lett.*, 2018, **9**, 2941–2945.
- 17 N. V. Teplakov, A. S. Baimuratov, I. A. Vovk, M. Y. Leonov, A. V. Baranov, A. V. Fedorov and I. D. Rukhlenko, *ACS Nano*, 2017, **11**, 7508–7515.
- 18 L. Protesescu, S. Yakunin, M. I. Bodnarchuk, F. Krieg, R. Caputo, C. H. Hendon, R. X. Yang, A. Walsh and M. V. Kovalenko, *Nano Lett.*, 2015, **15**, 3692–3696.
- 19 I. Lignos, V. Morad, Y. Shynkarenko, C. Bernasconi, R. M. Maceiczky, L. Protesescu, F. Bertolotti, S. Kumar, S. T. Ochsenbein, N. Masciocchi, A. Guagliardi, C.-J. Shih, M. I. Bodnarchuk, A. J. deMello and M. V. Kovalenko, *ACS Nano*, 2018, **12**, 5504–5517.
- 20 L. Protesescu, S. Yakunin, S. Kumar, J. Bär, F. Bertolotti, N. Masciocchi, A. Guagliardi, M. Grotevent, I. Shorubalko,

- M. I. Bodnarchuk, C.-J. Shih and M. V. Kovalenko, *ACS Nano*, 2017, **11**, 3119–3134.
- 21 H. Huang, M. I. Bodnarchuk, S. V. Kershaw, M. V. Kovalenko and A. L. Rogach, *ACS Energy Lett.*, 2017, **2**, 2071–2083.
 - 22 F. Liu, Y. Zhang, C. Ding, S. Kobayashi, T. Izuishi, N. Nakazawa, T. Toyoda, T. Ohta, S. Hayase, T. Minemoto, K. Yoshino, S. Dai and Q. Shen, *ACS Nano*, 2017, **11**, 10373–10383.
 - 23 G. Rainò, G. Nedelcu, L. Protesescu, M. I. Bodnarchuk, M. V. Kovalenko, R. F. Mahrt and T. Stöferle, *ACS Nano*, 2016, **10**, 2485–2490.
 - 24 M. A. Becker, R. Vaxenburg, G. Nedelcu, P. C. Sercel, A. Shabaev, M. J. Mehl, J. G. Michopoulos, S. G. Lambrakos, N. Bernstein, J. L. Lyons, T. Stöferle, R. F. Mahrt, M. V. Kovalenko, D. J. Norris, G. Rainò and A. L. Efros, *Nature*, 2018, **553**, 189–193.
 - 25 O. Pfingsten, J. Klein, L. Protesescu, M. I. Bodnarchuk, M. V. Kovalenko and G. Bacher, *Nano Lett.*, 2018, **18**, 4440–4446.
 - 26 G. Rainò, M. A. Becker, M. I. Bodnarchuk, R. F. Mahrt, M. V. Kovalenko and T. Stöferle, arXiv:1804.01873, 2018, ArXiv preprint.
 - 27 A. S. Baimuratov, A. I. Shlykov, W. Zhu, M. Y. Leonov, A. V. Baranov, A. V. Fedorov and I. D. Rukhlenko, *Opt. Lett.*, 2017, **42**, 2423–2426.
 - 28 A. S. Baimuratov, Y. K. Gun'ko, A. V. Baranov, A. V. Fedorov and I. D. Rukhlenko, *Sci. Rep.*, 2016, **6**, 23321.
 - 29 A. S. Baimuratov, I. D. Rukhlenko and A. V. Fedorov, *Opt. Lett.*, 2013, **38**, 2259–2261.
 - 30 A. S. Baimuratov, I. D. Rukhlenko, V. K. Turkov, A. V. Baranov and A. V. Fedorov, *Sci. Rep.*, 2013, **3**, 1727.
 - 31 F. Qiao, X. Wang, Q. Wang, G. He and Y. Xie, *Nanoscale*, 2017, **9**, 8066–8079.
 - 32 P. A. Crozier, J. Tolle, J. Kouvetakis and C. Ritter, *Appl. Phys. Lett.*, 2004, **84**, 3441–3443.
 - 33 T.-H. Kim, K.-S. Cho, E. K. Lee, S. J. Lee, J. Chae, J. W. Kim, D. H. Kim, J.-Y. Kwon, G. Amaratunga and S. Y. Lee, *et al.*, *Nat. Photonics*, 2011, **5**, 176–182.
 - 34 Y. L. Kong, I. A. Tamargo, H. Kim, B. N. Johnson, M. K. Gupta, T.-W. Koh, H.-A. Chin, D. A. Steingart, B. P. Rand and M. C. McAlpine, *Nano Lett.*, 2014, **14**, 7017–7023.
 - 35 R. J. Macfarlane, B. Lee, M. R. Jones, N. Harris, G. C. Schatz and C. A. Mirkin, *Science*, 2011, **334**, 204–208.
 - 36 A. S. Baimuratov, T. P. Pereziabova, W. Zhu, M. Y. Leonov, A. V. Baranov, A. V. Fedorov and I. D. Rukhlenko, *Nano Lett.*, 2017, **17**, 5514–5520.
 - 37 C. R. Kagan, E. Lifshitz, E. H. Sargent and D. V. Talapin, *Science*, 2016, **353**, aac5523.
 - 38 M. Yuan, M. Liu and E. H. Sargent, *Nat. Energy*, 2016, **1**, 16016.
 - 39 G. H. Carey, A. L. Abdelhady, Z. Ning, S. M. Thon, O. M. Bakr and E. H. Sargent, *Chem. Rev.*, 2015, **115**, 12732–12763.
 - 40 E. Busseron, Y. Ruff, E. Moulin and N. Giuseppone, *Nano-scale*, 2013, **5**, 7098–7140.
 - 41 J.-H. Im, C.-R. Lee, J.-W. Lee, S.-W. Park and N.-G. Park, *Nanoscale*, 2011, **3**, 4088–4093.
 - 42 Y. Tong, E.-P. Yao, A. Manzi, E. Bladt, K. Wang, M. Döblinger, S. Bals, P. Müller-Buschbaum, A. S. Urban, L. Polavarapu and J. Feldmann, *Adv. Mater.*, 2017, 1801117.
 - 43 Y. Kim, E. Yassitepe, O. Voznyy, R. Comin, G. Walters, X. Gong, P. Kanjanaboos, A. F. Nogueira and E. H. Sargent, *ACS Appl. Mater. Interfaces*, 2015, **7**, 25007–25013.
 - 44 V. M. Agranovich and V. L. Ginzburg, *Crystal Optics with Spatial Dispersion, and Excitons*, Springer, 2013.
 - 45 C. de Weerd, L. Gomez, H. Zhang, W. J. Buma, G. Nedelcu, M. V. Kovalenko and T. Gregorkiewicz, *J. Phys. Chem. C*, 2016, **120**, 13310–13315.
 - 46 V. M. Agranovich, *Excitations in Organic Solids*, Oxford University Press, 2009.
 - 47 H. Haug and S. W. Koch, *Quantum Theory of the Optical and Electronic Properties of Semiconductors*, World Scientific Publishing, 2009.
 - 48 M. Fu, P. Tamarat, H. Huang, J. Even, A. L. Rogach and B. Lounis, *Nano Lett.*, 2017, **17**, 2895–2901.
 - 49 C.-H. Park, L. Yang, Y.-W. Son, M. L. Cohen and S. G. Louie, *Nat. Phys.*, 2008, **4**, 213–217.
 - 50 E. M. Lifshitz and L. P. Pitaevskii, *Statistical Physics: Theory of the Condensed State*, Elsevier, 2013.
 - 51 M. Born and K. Huang, *Dynamical Theory of Crystal Lattices*, Clarendon Press, 1954.